Monthly Notices
of the
ROYAL ASTRONOMICAL SOCIETY

MNRAS **485,** 1614–1625 (2019)
Advance Access publication 2019 January 29

doi:10.1093/mnras/stz283

The PDS 110 observing campaign – photometric and spectroscopic observations reveal eclipses are aperiodic

H. P. Osborn,[1]† M. Kenworthy,[2] J. E. Rodriguez,[3] E. J. W. de Mooij,[4] G. M. Kennedy,[5,6] H. Relles,[7] E. Gomez,[7] M. Hippke,[8] M. Banfi,† L. Barbieri,† I. S. Becker,[9] P. Benni,[10]† P. Berlind,[3] A. Bieryla,[3] G. Bonnoli,[11] H. Boussier,† S. M. Brincat,† J. Briol,† M. R. Burleigh,[12] T. Butterley,[13] M. L. Calkins,[3] P. Chote,[5] S. Ciceri,[14] M. Deldem,† V. S. Dhillon,[15,16] E. Dose,† F. Dubois,[17]† S. Dvorak,† G. A. Esquerdo,[3] D. F. Evans,[18] S. Ferratfiat,† S. J. Fossey,[19,20] M. N. Günther,[21] J. Hall,† F.-J. Hambsch,[22]† E. Herrero,[23] K. Hills,† R. James,† R. Jayawardhana,[24] S. Kafka,[25] T. L. Killestein,[4]† C. Kotnik,† D. W. Latham,[3] D. Lemay,† P. Lewin,† S. Littlefair,[15] C. Lopresti,† M. Mallonn,[26] L. Mancini,[27,28,29] A. Marchini,[11]† J. J. McCormac,[5,6] G. Murawski,[30]† G. Myers,[25] R. Papini,† V. Popov,[31]† U. Quadri,† S. N. Quinn,[3] L. Raynard,[12] L. Rizzuti,† J. Robertson,[32] F. Salvaggio,† A. Scholz,[33] R. Sfair,[9] A. M. S. Smith,[34] J. Southworth,[18] T. G. Tan,[35]† S. Vanaverbeke,[17]† E. O. Waagen,[23] C. A. Watson,[36] R. G. West,[5,6] O. C. Winter,[9] P. J. Wheatley,[5,6] R. W. Wilson[13] and G. Zhou[3]

Affiliations are listed at the end of the paper

Accepted 2019 January 23. Received 2019 January 23; in original form 2018 June 22

ABSTRACT

PDS 110 is a young disc-hosting star in the Orion OB1A association. Two dimming events of similar depth and duration were seen in 2008 (WASP) and 2011 (KELT), consistent with an object in a closed periodic orbit. In this paper, we present data from a ground-based observing campaign designed to measure the star both photometrically and spectroscopically during the time of predicted eclipse in 2017 September. Despite high-quality photometry, the predicted eclipse did not occur, although coherent structure is present suggesting variable amounts of stellar flux or dust obscuration. We also searched for radial velocity (RV) oscillations caused by any hypothetical companion and can rule out close binaries to $0.1 M_{\rm s}$. A search of Sonneberg plate archive data also enabled us to extend the photometric baseline of this star back more than 50 yr, and similarly does not re-detect any deep eclipses. Taken together, they suggest that the eclipses seen in WASP and KELT photometry were due to aperiodic events. It would seem that PDS 110 undergoes stochastic dimmings that are shallower and of shorter duration than those of UX Ori variables, but may have a similar mechanism.

Key words: protoplanetary discs – stars: individual:PDS 110 – stars: variables: T Tauri, Herbig Ae/Be.

1 INTRODUCTION

In the process of planet formation, a circumstellar disc is formed around a star. This circumstellar disc, and the subsequent formation of protoplanetary cores, can be probed and studied by direct imaging, but also through photometric observations of young stars.

* E-mail: hugh.osborn@lam.fr
† AAVSO contributor.

Protoplanetary cores subsequently draw matter from the circumstellar disc, potentially forming a circumplanetary disc that fills a significant fraction of the Hill sphere of the planet (e.g. see reviews by Armitage 2011; Kley & Nelson 2012), which accretes either on to the exoplanet, into exo-moons, or possibly exo-rings (Canup & Ward 2002; Magni & Coradini 2004; Ward & Canup 2010). Such objects can also be probed through either direct imaging of young planets (e.g. Ginski et al. 2018; Vanderburg, Rappaport & Mayo 2018), or through photometric observations as they transit their host star (e.g. Heising, Marcy & Schlichting 2015; Aizawa et al. 2018; Teachey, Kipping & Schmitt 2018). One such candidate is the young star 2MASS J14074792-3945427 ('J1407') that underwent a complex eclipse two months in duration that was interpreted as the transit of a highly structured ring system filling the Hill sphere (Mamajek et al. 2012; Kenworthy & Mamajek 2015). In the case of planetary companions, transit photometry and spectroscopy of such a Hill sphere system provide the opportunity to probe both the spatial and chemical composition of a circumplanetary disc during planetary formation.

Alternatively, circumstellar material can also periodically eclipse young stars, allowing us to probe stochastic processes in protoplanetary discs. Many young stars have been observed to display such 'dipper' behaviour (Bouvier et al. 1999; Cody & Hillenbrand 2014; Ansdell et al. 2016, 2018, etc.), and proposed explanations include the transit of accretion streams (Bouvier et al. 1999), material from asteroid collisions (Kennedy et al. 2017), coalescing circumstellar dust clumps (Rodriguez et al. 2013), etc.

PDS 110 (HD 290380) is a young (∼11 Myr old) T-Tauri star in the Orion OB1 Association that showed two extended (2 week) eclipses (30 per cent) in 2008 and 2011, separated by a delay of 808 d. An analysis by Osborn et al. (2017) of all known photometry was consistent with an unseen companion in a periodic orbit of 808 d with a predicted 3-week long eclipse occurring around 2017 September, although aperiodic UX Ori-like dimmings could not be ruled out. If periodic, the resulting ephemeris predicted two eclipses to have already occurred (in 2013 and 2015), however, due to the unfavourable placement of PDS 110 during this season, they were not observed by any photometric survey. An observable eclipse was predicted at HJD = 2458015.5 ± 10 (1σ region 2017 Sept 9–30) with a full width at half-maximum of 7 ± 2 d.

In Section 2, we present photometry from a coordinated campaign[1] to provide high cadence photometric measurements during the period from 2017 August into early 2018.[2]

In Section 3, we detail further high-resolution spectroscopic observations obtained with TRES at the Whipple Observatory, and UVES on the VLT. In Section 4, we detail the analysis of nearly 40 yr of photographic plates carrying out an archival search for other eclipse events. With Section 5 and in the Conclusions, we speculate what caused the observed eclipses and suggest future observations of PDS 110.

2 2017 PHOTOMETRIC OBSERVATIONS

Photometric observations were taken by 11 professional observatories, with dozens more professional and amateur observers contributing through AAVSO. These spanned 10 different optical filters including SDSS ugriz and Cousins BVRI filters, as well as the broad-band NGTS filter. The majority of observations began around 2457 980 (2017 August 15) and finished once the time of predicted eclipse had past (2458 090, or 2017 December 3). These are summarized in Fig. 1. Some observations (from NGTS and AAVSO) continued into 2018, with a small part of that extended time frame shown in Fig. 3.

In the following section, we briefly summarize the observations of each contributing observatory.

2.1 Contributing observatories

2.1.1 Las Cumbres Observatory

Las Cumbres Observatory (LCOGT) is a global network of robotic telescopes perfectly suited to the continuous, median-cadence observations required to detect long-duration dimmings of young stars. Under the proposal 'Characterization of the eclipsing body orbiting young star PDS 110' (LCO2017AB-003), we were granted 35 hr of time on the 0.4 m network. This consists of 10 identical 0.4 m Meade telescopes at six LCOGT observatory nodes: Siding Spring Observatory in Australia, Teide Observatory on Tenerife, McDonald Observatory in Texas, Cerro Tololo in Chile, South African Astronomical Observatory (SAAO) in Sutherland, South Africa, and Haleakala Observatory in Hawai'i. These have a 2000 × 3000 SBIG STX6303 camera with a 14-position filter wheel including Sloan $u'g'r'i'z'$, and Johnson/Cousins V and B. We primarily used 0.4 m time to observe in Sloan $g'r'i'z'$.

We were also assisted in these efforts by the observing campaign 'Time-Domain Observations of Young Stellar Objects' (STA2017AB-002, PI: Aleks Scholz), which contributed 10 hr of time on the 1 m LCOGT network. This includes telescopes at McDonald Observatory, Cerro Tololo, SAAO, and Siding Spring Observatory. These have a 4k × 4k Sinistro camera and 24 filter options including Johnson/Cousins *UBVRI* and Sloan $u'g'r'i'$. We primarily used the 1 m time to observe PDS 110 in Johnson/Cousins *BVRI* and Sloan *u* (where PDS 110 is faintest).

In both 1 m and 0.4 m time, we took observing blocks of three images in each filter around three times per day, with exposure times adjusted to achieve signal-to-noise ratio (SNR) ≈ 200. The data were accessed via the online observing portal, and the images and calibration files downloaded. AstroImageJ was then used to perform the calibrations and the reference photometry using the reference stars provided by AAVSO.

2.1.2 AAVSO

AAVSO is an international organization designed to connect any observers capable of high-quality photometric observations (including amateurs) with astronomical projects, which require observations (Kafka 2016). An AAVSO Alert notice was released to observers (alert 584, Waagen 2017),[3] which included a list of comparison stars, and more than 30 observers submitted observations during the campaign.

2.1.3 NITES, La Palma

The Near Infra-red Transiting ExoplanetS (NITES) telescope is a 0.4 m, f/10 Meade telescope located at the Observatorio del Roque de los Muchachos on La Palma, and equipped with an e2v, 1024 × 1024 CCD with an FoV of 11.3 × 11.3 arcmin (McCormac

[1] Co-ordinated at http://pds110.hughosborn.co.uk.
[2] All photometry of PDS110 is available as supplementary material.
[3] https://www.aavso.org/aavso-alert-notice-584

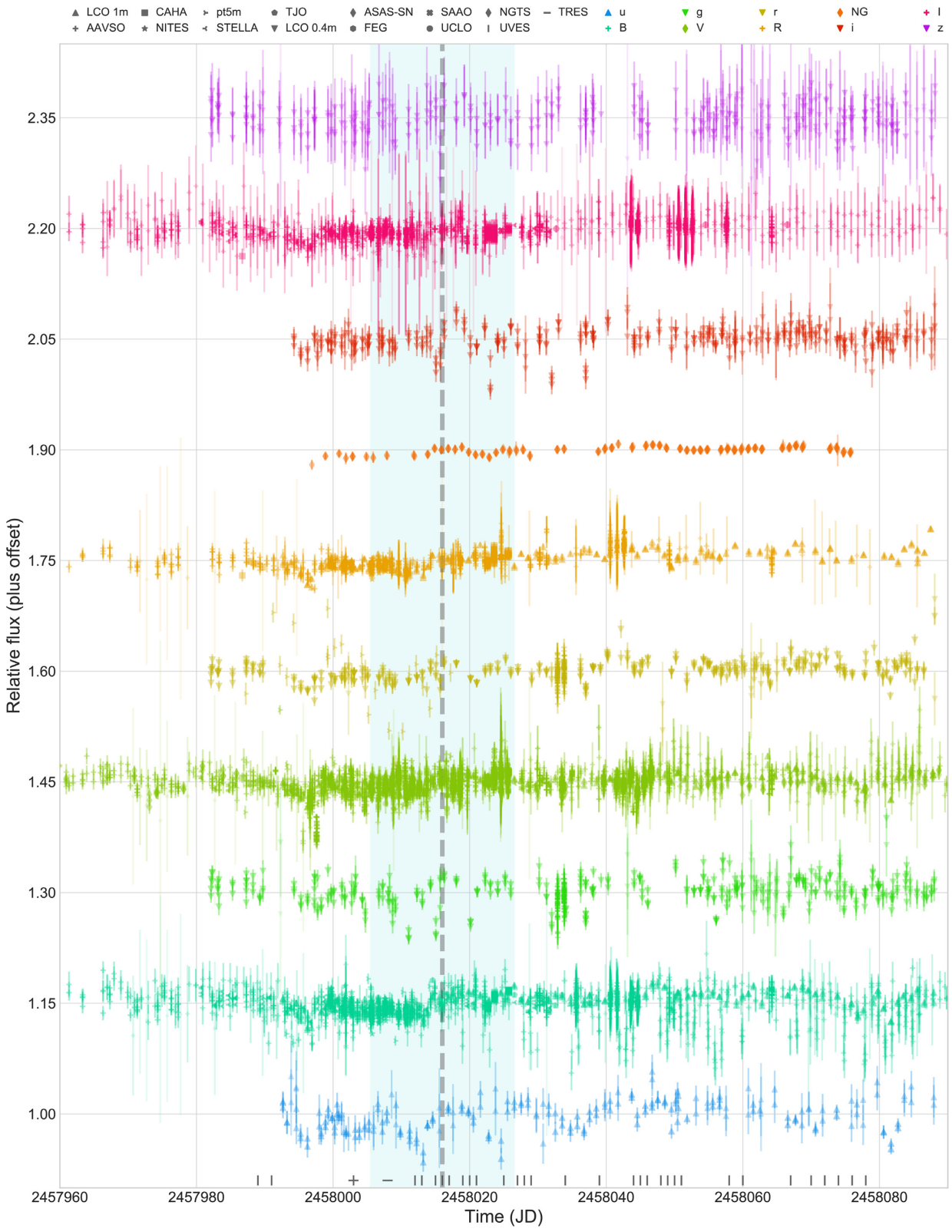

Figure 1. Photometry of PDS 110 from JD = 2457 960 to 2458 090, or 2017 July 25 to 2017 December 2. Telescopes used are shown using marker shape, while filters are shown by colour and flux offset (with blue to red from bottom to top). *ugriz* filters correspond to Sloan primed bandpasses. *UBVRI* are Johnson/Cousins. Epochs of spectroscopic observations are shown at the base of the plot as vertical (VLT/UVES) and horizontal (TRES) lines. The transparency is dictated by the SNR, with points with large error bars made fainter. The filled vertical region shows the predicted time of central eclipse from Osborn et al. (2017) with the boundary corresponding to 1σ uncertainties. Some observations continued into 2018 and are shown in Fig. 3.

et al. 2014). NITES observed PDS 110 in four filters (Johnson *BVRI*) during 7seven nights between JD = 2457 999 and JD = 2458 011. The McCormac et al. (2013) 'DONUTS' system enabled accurate autoguiding.

2.1.4 STELLA, Tenerife

STELLA is composed of two 1.2 m robotic telescopes at the Izana Observatory on Tenerife, Spain (Strassmeier et al. 2004), which focuses on long-term photometric and spectroscopic monitoring of stellar activity (e.g. Mallonn et al. 2018). The wide-field imager, WiFSIP, has a 22 × 22 arcmin FoV and took observations of PDS 110 four times per night in *B*, *V,* and *I* filters (Johnson) with exposure times of 20, 12, and 10 s. We obtained data on 38 nights from 2017 August to October. The data reduction and extraction of the differential photometry of the target followed the description in Mallonn et al. (2018). We used `SExtractor` for aperture photometry and employed the same comparison stars for the three broad-band filters.

2.1.5 NGTS, Chile

Next-Generation Transit Survey (NGTS) is composed of 12 × 20 cm telescopes, each observing 8.1 deg^2 (2.8 × 2.8 deg^2) of the sky with a wide-band filter (from 520 to 890 nm) and a 2048 × 2048 deep-depleted CCD. Its primary goal is to achieve mmag-precision photometry in order to search for transiting exoplanets (Wheatley et al. 2018). Between Julian dates 2457 997 and 2458 199, PDS 110 was included in one of the NGTS survey fields and continuously observed by a single camera while above 30° elevation. A of total of 95 nights of data were collected, with a typical hourly RMS below 1 per cent. The raw 10 s NGTS frames were processed using a custom reduction pipeline (Chote, in preparation) to extract aperture photometry using several nearby comparison stars. The data were binned to 1 hr bins before being included with the other photometric data here.

2.1.6 CAHA 1.23m, Calar Alto

Remote observations enabled 251 images of PDS 110 to be taken from the Calar Alto 1.23 m telescope. This robotic telescope has a DLR Mk3 CCD, which observed in *BVRI* Johnson filters. Aperture photometry was performed with DEFOT (see Southworth et al. 2009, 2014) for PDS 110 with three comparison stars providing relative photometry.

2.1.7 ASAS-SN

The All Sky Automated Survey for SuperNovae (ASAS-SN; Shappee et al. 2014; Kochanek et al. 2017) is a 20-unit network of wide-field telescopes designed to survey the entire sky in *ugriz g* magnitude down to magnitude 17 each night, with the primary goal of rapidly detecting supernovae. We accessed ASAS-SN data of PDS 110 data from the Sky Patrol search page.[4]

[4]https://asas-sn.osu.edu/

2.1.8 FEG, Sao Paulo

Observations were carried out with a 16-in Meade LX200 telescope and a Merlin EM247 camera, with *V*-band filter and exposure time of 5 s. Useful data were acquired between 2017 September 2 and 29, totaling 5397 images in 14 nights.

Each one of the 660 × 498 pixels frames was calibrated by bias subtraction and flat-field correction. The fluxes of the target and nearby stars were determined from each image through aperture photometry taking advantage of the routines provided by the IDL Astronomy Library. The magnitude was calculated using the comparison stars provided by AAVSO (usually 000-BMH-803), with an error of 0.01 mag.

To determine the time evolution of the magnitude, the data were averaged every 36 images (3 min cadence), avoiding any spurious variation due to instrumental or meteorological effects.

2.1.9 TJO, Montsec Astronomical Observatory

PDS 110 was observed with the Joan Oró robotic 0.8 m telescope (TJO) at the Montsec Astronomical Observatory in Catalonia. The TJO is equipped with Johnson/Cousins *UBVRI* filters and an e2v 2*k* × 2*k* CCD with an FoV of 12.3 × 12.3 arcmin. Johnson *B* and *I* filters were used and several observing blocks per night with five exposures each were configured. The exposure times for each filter were adjusted in order to achieve SNR ≈ 300. The images were reduced using the ICAT reduction pipeline at the TJO (Colome & Ribas 2006) and differential photometry was extracted using AstroImageJ. The final TJO data set contains 255 and 225 data points in the *B* and *I* filters, respectively, taken in 20 different nights between September 5 and October 9.

2.1.10 pt5m, La Palma

pt5m is a 0.5 m robotic telescope located at the Roque de los Muchachos Observatory, La Palma (Hardy et al. 2015). It observed PDS 110 on 21 separate nights between JD = 2457 993 and 2458 015 in Johnson *B*, *V,* and *R* filters. Astrometry was performed automatically on all images by cross-matching detected sources against the 2MASS point-source catalog. Instrumental magnitudes were calculated for all detected objects in the images using `SExtractor`. Instrumental magnitudes for the *B* and *V* observations were calculated using zero-points derived by cross-matching against the APASS (AAVSO Photometric All-Sky Survey) catalogue, whilst a cross-match against catalogued SDSS-r' magnitudes gave a zero-point for the *R*-band images. No colour terms were applied.

2.1.11 SAAO

The SAAO 1 m was used on two nights to observe PDS 110 in three bands using a Sutherland high-speed optical camera (Coppejans et al. 2013). However, the small field of view (2.85 × 2.85 arcmin) made reference stars difficult, and the reduction required the use of measurements submitted by other observatories for calibration. The high-cadence data (cadence from 0.7 to 10 s) allowed a search for short-period oscillations ($P < 3d^{-1}$), however, none were detected. The data were binned with a weighted mean to 7.2-min bins before being included in the ensemble analysis.

2.1.12 UCL Observatory

PDS 110 was observed on 11 separate nights between JD 2457 996 and 2458 165 from the University College London Observatory (UCLO), located in Mill Hill, London. A fully robotic 0.35-m Schmidt Cassegrain was used with an SBIG STL-6303E CCD camera. Observations were taken in Astrodon R_c and I_c (Cousins) filters (for more observing details, see Fossey, Waldmann & Kipping 2009). Typically, 10–30 exposures of 20 s were obtained in each filter on each night; differential photometry relative to an ensemble of nearby comparison stars yielded a total of 230 measurements in R_c and 150 in I_c, binned to provide average relative fluxes on nine nights for each filter.

2.2 Photometric ensemble analysis

With any observing campaign involving the inclusion of photometry between multiple observatories across multiple filters, the pooling and comparison of data are a difficult task. Each observer introduces their own systematics, including most visibly an offset in the magnitude or normalized flux level. This is despite, in some cases, using identical filters and the same comparison stars.[5] In the case of our PDS 110 campaign, however, the precise magnitude measurements are not as important as the relative change overtime. Therefore, we applied an offset to each light curve to enable comparisons between them, using the long baseline and high accuracy of the LCOGT photometry as a guide. In the case where light curves were provided with normalized flux, we converted these to differential magnitudes taking the archival magnitude as the whole light-curve flux median before assessing the offsets.

The potential low-level variability of PDS 110 and the large variations in observation cadence between observations mean that simply adjusting the medians of data in a certain region is not ideal. Instead, we developed a minimization process that computes the sum of the magnitude difference between each point on one light curve and each point on another ($y_{a,i}-y_{b,j}$ in equation (1) where y is magnitude and a and b represent two photometry sources). This is then weighted for the time separation between those points ($x_{a,i}-x_{b,j}$ in equation (1), where x is time in days). In an effort to remove the influence of a structured light curve combined with irregular time sampling, we weighted the magnitude difference between points by the absolute time difference between them, scaled using a squared exponential and a length-scale (l) of 4 d. The minimization function ($f_{\rm min}$) is defined in equation (2.2):

$$f_{\rm min} = \sum_{i=1}^{N_a}\sum_{j=1}^{N_b} \frac{\left(y_{a,i} - (y_{b,j} + \Delta_m)\right)^2}{\sigma_{a,i}^2 + \sigma_{b,j}^2} \exp \frac{-(x_{a,i} - x_{b,j})^2)}{2l^2}. \quad (1)$$

Bootstrapping was performed to assess the increase in errors due to this method, which were added in quadrature to the flux of the adjusted points. This procedure was then performed iteratively on each data set in each filter until the offsets converged, with the exception of our LCOGT data (and CAHA data in I band), which we held as a fixed reference light curve. The result is a magnitude offset (Δm) and uncertainty for each filter, and for each telescope. NGTS data were not minimized in this way as it observed in a unique broad-band filter.

The computed offsets for each telescope, which have been converted to relative flux to match the light curves presented in the following figures, are shown in Table A1 and A2. They show

[5]Provided by AAVSO

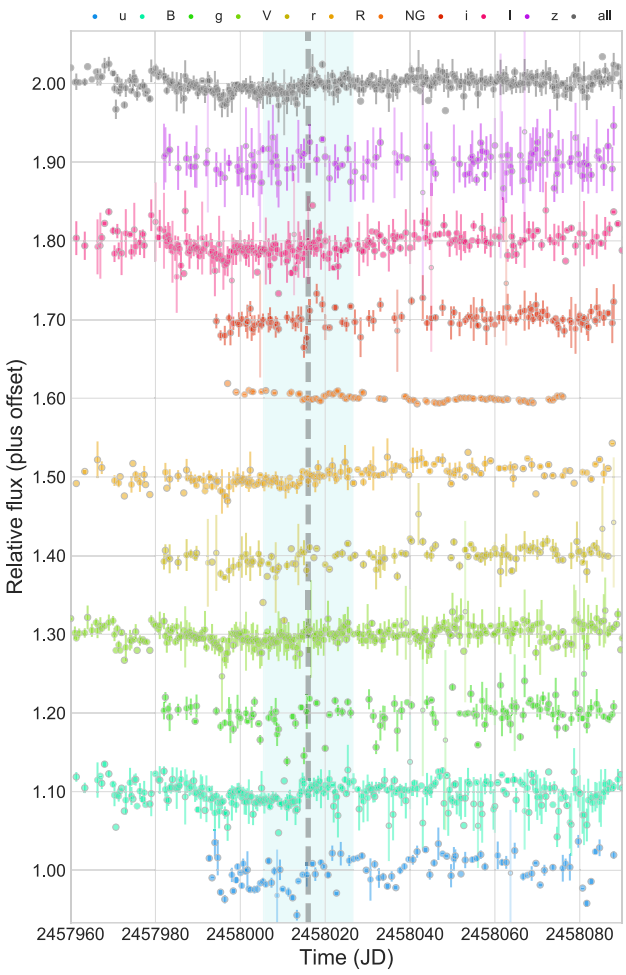

Figure 2. Photometry of PDS 110 binned into 0.333 d time bins for each filter and spanning the same time period as Fig. 1. The combined light curve for all filters is shown above in grey.

good agreement for the B and V band, but large negative shifts in relative flux for R and I, suggesting a disagreement between the historic R- (Zacharias et al. 2003) and I-band values (Epchtein et al. 1994), which the baseline LCOGT data were adjusted to. However, as we are focused on the change in time, these variations are unlikely to cause significantly increased systematics.

Full photometry for PDS 110 during the campaign is shown in Fig. 1. We also release all data publicly as supplementary material to this publication.

2.3 Observed candidate dimming events

Two significant dimming events were observed, although their occurrences are inconsistent with the prediction from previous dimmings, in terms of both timing and depth. The first was before the predicted time of eclipse at JD ∼ 2457 996 in all bands (visible in the binned photometry in Fig. 2). It lasted less than 1 d and saw flux dip by only ∼5 per cent, so does not resemble the previously reported events.

A second dimming event was seen after the official end of the campaign in 2018 with a centre at JD = 2458 186 (see Fig. 3). Similarly, its shape is for the most part inconsistent with the previously observed dimmings – it is both far weaker and of

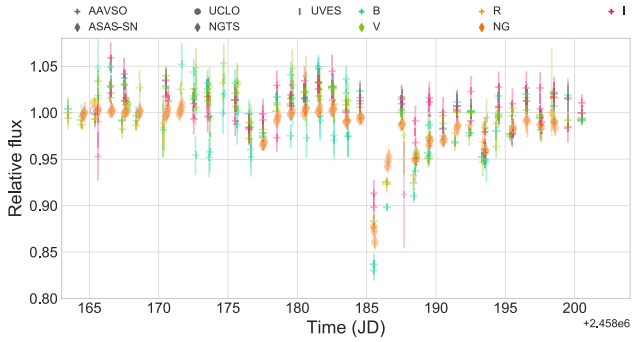

Figure 3. Photometry (with no flux offset) of the short-duration eclipse seen in 2018.

shorter duration, with only a single night showing a depth, $\delta >$ 10 per cent. While the NGTS data show the event clearest, it was also observed by AAVSO observers and ASAS-SN. These also show that shallower dips (of ∼4 per cent) occurred ∼8 d before and afterwards.

These two events appear to suggest that more rapid time-scale dimmings are possible than expected from Osborn et al. (2017), and may suggest the single-night flux drops observed in ASAS data in 2006 and 2007 may have also been real rather than, as speculated in Osborn et al. (2017), anomalous flux values.

2.4 Reddening

Obscuration of the star by small dust causes more light to be blocked by dust grains close in size to the wavelength of light. Hence, typically, dips appear deeper in blue filters than in red. Although no major dips were observed, short duration and shallow depth variability seen in PDS 110 may be enough to spot the imprint of dust. In Fig. 4, we explore this by plotting the difference in magnitude of the binned *V*-band light curve (our most well-covered filter) and the photometry from other filters taken at the same time. Lines of best fit are plotted using the `bces` package[6] and three assumptions detailed in the figure caption (Nemmen et al. 2012). We see that the gradient in the *u* band appears far steeper than would be expect for a 'grey' absorber. Intriguingly, the *I*-band observations also show a steeper-than-grey correlation, especially due to brighter-than-average points. This remains unexplained and appears to contradict the effect of reddening. Systematics, especially for the low-SNR photometric observations in the *I* band, would appear the most likely cause.

However, correlations are also likely present due to telescope-specific systematics across all bands and times, which would similarly manifest as a positive correlation between filters. This may be responsible for why *BRI* filers show stronger correlations to *V* band than *ugriz* filters (which were typically not observed contemporaneously as *V*). Therefore, we choose not to model the reddening present in all observations, although we note that dust may be present. Exploring the extinction or dust grain analysis of single dips (e.g. that in Fig. 3) is also problematic due to the lack of perfectly simultaneous data and uncorrected systematic offsets between telescopes.

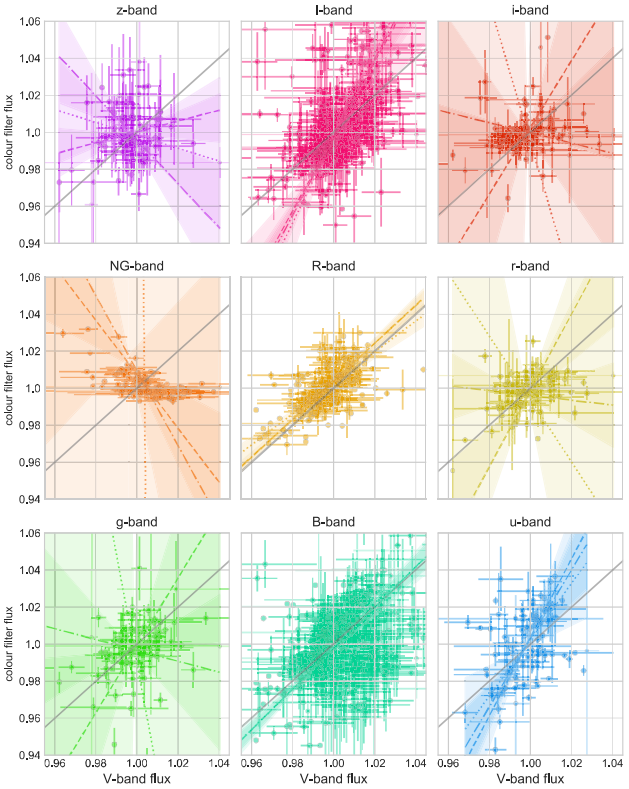

Figure 4. Flux correlations for each binned filter values compared to *V* band. Points along the diagonal line (shown in grey) would represent dimmings perfectly correlated with *V*-band flux (and therefore 'grey'). Lines of best fit are computed using `bces` and 'Orthogonal least squares' (dashed), Vmag as the independent variable (dotted), and the bissector method (dash–dotted). 1σ error regions for each are overplotted.

3 HIGH-RESOLUTION SPECTROSCOPY

3.1 TRES

Using the Tillinghast Reflector Echelle Spectrograph (TRES; Fűrész 2008)[7] on the 1.5 m telescope at the Fred Lawrence Whipple Observatory on Mount Hopkins, AZ, we observed PDS 110 nine times from UT 2016 Oct 09 until UT 2017 Sep 11. The spectra were taken with a resolving power of $\lambda/\Delta\lambda \equiv R = 44\,000$ covering a wavelength range of 3900–9100 Å. For each order, we cross-correlate each spectrum against a template made from all median-stacked spectra that is aligned to that with the highest S/N. To derive the relative RVs, we fit the peak of the cross-correlation function across all orders. The scatter between each order for each spectrum determines the uncertainties on the relative RVs (Buchhave et al. 2010). Activity and rotation mean that the resulting relative RVs give a uniform offset from that initial high-S/N spectra therefore we re-adjust the RVs to be self-consistent. We also performed a fit simply using the strongest observed spectra as a template, which gives consistent results but with slightly lower precision.

We see no large variation (>1 km s^{-1}) in the TRES radial velocity measurements. We note that since PDS 110 is a late-F star with broad lines due to a projected equatorial rotational velocity of 60 km s^{-1}, precise radial velocities are challenging. Our observations cover the

[6] https://github.com/rsnemmen/BCES

[7] http://www.sao.arizona.edu/html/FLWO/60/TRES/GABORthesis.pdf

Table 1. TRES relative radial velocity measurements.

BJD_{TDB}	RV (km s^{-1})	σRV (km s^{-1})
2457 670.989 05	− 0.32	0.35
2457 679.987 38	− 0.98	0.45
2457 685.000 57	− 1.02	0.37
2457 786.707 41	0.00	0.38
2457 800.695 17	0.15	0.43
2457 823.720 00	− 1.22	0.42
2457 855.632 04	− 0.46	0.33
2458 002.985 22	− 0.90	0.58
2458 007.985 72	0.10	0.27

first half of the predicted orbital period from Osborn et al. (2017) with a standard deviation from the mean of 0.53 km s^{-1}. Using a 3σ value as the upper limit (1.59 km s^{-1}), assuming a 1.6 $M_\odot$ host star, and fixing the orbit to that of the predicted ephemeris (T_C = 2454 781, P = 808.0 d) from Osborn et al. (2017), this would correspond to an upper mass limit for the companion of ∼100 M_{Jup}. We also run a Levenberg–Marquardt fit to the RVs, enforcing the ephemeris and a circular orbit, and get a 3σ upper limit on the mass of 68 M_{Jup}. However, these upper limits make the assumption that we know the ephemeris of the companion. The RV measurements from TRES are shown in Table 1 .

3.2 UVES

High spectral resolution observations of PDS 110 were obtained with the Ultraviolet and Visible Echelle Spectrograph (UVES; Dekker et al. 2000) on the Very Large Telescope (VLT) in Chile as part of the DDT programme 299.C-5047 (PI: De Mooij) on 32 nights between 2017 August 24 and November 21.

Using the #2 Dichroic, the spectra on every night were obtained using both the blue and red arms simultaneously with the 437 + 760 nm wavelength setting. Using this set-up, the blue arm covers a wavelength range from ∼3730 to ∼5000 Å, while the red arm has a wavelength coverage from ∼5650 to ∼9560 Å, with a small gap between the two CCDs that make up the red array. In this paper, however, for the red arm we only use the shorter wavelength CCD, as this is less affected by telluric lines. The blue arm is not affected by telluric lines. During each visit, a total of four spectra were obtained, each with an exposure time of 300 s.

The data were reduced using the ESO UVES pipeline version 5.7.0 through ESO Reflex. The pipeline reduced and merged spectra from each epoch were combined to increase the SNR. As the wavelength range of the red arm of UVES contains strong telluric bands (including the O_2 bands), we first used the ESO Molecfit tool[8] (Smette et al. 2015) to correct the spectra for telluric absorption.

The observations were corrected for blaze variations from epoch to epoch, by first dividing the spectra from each epoch by the spectrum of the first epoch, binning this ratio, interpolating it using a cubic spline, and finally dividing the spectra by the interpolated function. This was done for each of the arms separately. A master spectrum was generated by averaging the blaze-corrected spectra from individual nights, and the envelope was used to create a continuum normalization that was then applied to all spectra. Finally, we used least-squares deconvolution, based on Donati et al.

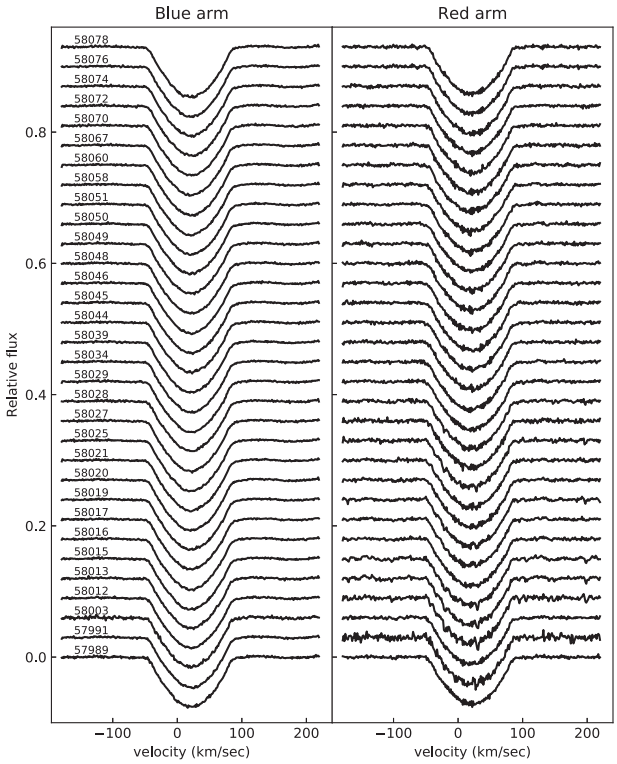

Figure 5. Least-squares deconvolution line profiles of the UVES observations of PDS 110. The Julian dates for the start of the night are indicated above each profile. The left-hand panel shows the profiles for the blue arm of UVES, while the right-hand panel shows the same for the red arm.

(1997) as implemented by Watson, Dhillon & Shahbaz (2006), to combine the signal from the multiple stellar lines and increase the SNR. Care was taken to mask both bands with strong telluric residuals (e.g. the saturated O_2 bands in the red arm) as well as wavelength regions that are strongly affected by stellar emission features (e.g. the Balmer lines, Ca II H&K lines, the Na D lines) due to accretion. The line list of ∼2400 lines was generated using the 'Extract Stellar' option from the VALD3 data base (Ryabchikova et al. 2015)[9] for the stellar parameters from Osborn et al. (2017). The resulting Least-Squares Deconvolution (LSD) profiles for the red and blue arms are shown in Fig. 5. In Fig. 6, we show the differences between the individual line profiles and the median line profile taken over the entire UVES observing campaign. Structure transiting the stellar disc (e.g. a ring-crossing event) would induce a bump in the (residual) line profile where light from the stellar surface at a certain Doppler shift is occulted, (which causes the Rossiter–McLaughlin effect, e.g. de Mooij, Watson & Kenworthy 2017), however, no such signature is observed. A detailed study of the emission lines, which show information about the accretion rate, the inclination of the star, etc, will be included in a future analysis (de Mooij et al., in preparation).

4 PLATE PHOTOMETRY 1956–1994

The second largest plate archive in the world, after Harvard (which is yet to digitize data from PDS_110) is located at Sonneberg Observatory (Bräuer & Fuhrmann 1992). Two observation programs

[8] https://www.eso.org/sci/software/pipelines/skytools/molecfit

[9] http://vald.astro.uu.se/

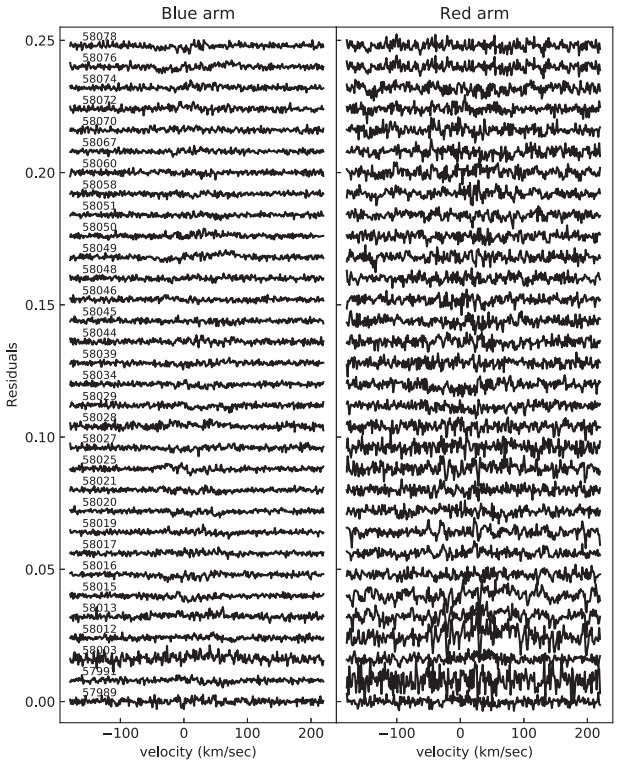

Figure 6. Differences of the line profiles shown in Fig. 5 compared to the median line profile over the entire UVES observing campaign.

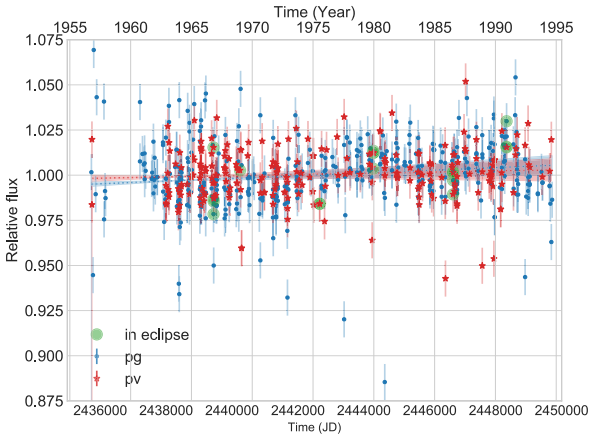

Figure 7. Sonneberg plate archival photometry from 1956 to 1994 in *pg* (blue) and *pv* (red) filters. We use the point-to-point median absolute difference (∼1 per cent) as a global uncertainty, as individual measurement uncertainties are typically underestimated and likely systematics dominated. The points circled represent those predicted to be in eclipse using the ephemeris of Osborn et al. (2017). The dashed orange and blue lines show 1D polynomial trends, and the filled regions show the 1σ error cones for each .

contributed 275 000 plates between 1935 and 2010 in two colour bands, *pg* (blue) and *pv* (red) (Bräuer et al. 1999). We use the Sky Patrol plates of 13 × 13 cm^2 size, a scale of 830 arcsec mm^{-1}, giving a field size of about 26 × 26 deg^2, taken between 1935 and 1994. The limiting magnitudes are of order 14.5 mag in *pg* and 13.5 mag in *pv*. Plates were scanned at 15 μm with 16 bit data depth. Typical exposure times are 30–60 min.

Our reduction pipeline is described in depth in Hippke et al. (2017). In brief, we perform an astrometric solution (Lang et al. 2010) using a list of coordinates of the brightest sources as an input and the Tycho-2 catalogue as a reference. With the source coordinates, we perform photometry using the `SExtractor` program (Bertin & Arnouts 1996) with a constant circular aperture.

As quality filters, we remove plates with suboptimal astrometric solutions, and those with bad quality after visual examination, which included all plates between 1936 and 1956, potentially to plate degradation. For calibration, we used the 10 nearest stars between magnitude 10 and 12, as recommended by the AAVSO observation campaign. After calibration, the average standard deviation of the magnitudes is ∼0.05 mag, significantly better than the ∼0.1 mag obtained on plates for dimmer stars (e.g. Collazzi et al. 2009; Goranskij et al. 2010; Johnson et al. 2014). We attribute the better quality to stricter quality cuts, the higher brightness of the star, and its location near the plate centre on many plates.

We show the time-series photometry in Fig. 7, where the blue and red symbols represent the photometric bands. Our good data cover JDs 2435 730 to 2449 710, or dates between 1956 September 14 and 1994 December 24. There are no obvious dimmings in the time series, with the darkest measurement ∼10 per cent below the mean. No significant long-term trend is detected in either filter (trends are 7.5 ± 2.3 × 10^{-9} and 3.3 ± 2.8 × 10^{-9} yr^{-1} in *pg* and *pv*, respectively), suggesting the brightness of PDS 110 is stable on the order of decades.

When we phase-fold the data to a period of 808 d, a handful of data points is near (within 15 d of) the expected eclipse, as shown in Fig. 7. In no case, do we see any indication of a dip.

5 DISCUSSION

The ephemeris predicted in Osborn et al. (2017) relied on the detection of two bona fide dips, plus a lack of corroborating photometry at other predicted eclipse times. However, the photometry collected by our campaign reveals no dip with a depth greater than ∼1 per cent during the predicted ephemeris (HJD = 2458 015.5 or 2017-09-20 ± 10 d). One potential solution to the lack of an event may be that the orbit of the body has decayed such that the eclipse was missed. However, extensive pre-dip data in 2013 (e.g. with KELT and ASAS-SN photometry), the archive photometry from Sonneberg plates, and the long baseline of the 2017 observations help rule out this hypothesis.

Such a rapid movement of large dust structures on the time-scale of only a few orbits would contradict the hopeful hypothesis of Osborn et al. (2017), which postulated long-lived dust encircling a periodic giant planetary or low-mass stellar object. The absence of an RV signature (albeit in noisy, rotation-dominated data) also points away from any hypothesis involving a high-mass companion. In sum, we no longer have substantial proof of PDS 110's periodicity and the data are more consistent with an aperiodic explanation.

The presence of other smaller (and shorter duration) dips, two of which were observed during the 2017–2018 observing campaign (see Figs 2 and 3), and some of which were hinted at in ASAS 2006 observations, also suggest an aperiodic cause. The low-flux points seen in archival Sonneburg photometry (see Fig. 7) may also be the result of bona fide short-duration dipping events, unresolved due to the ∼few day cadence of those observations.

PDS 110 is encircled by a large dust disc, as revealed in the IR observations, and this dust is likely the source of any deep and short-duration variability. The lack of reddening suggests we are observing PDS 110 high above the disc plane, and therefore some

mechanism must exist to get clumps of material into our line of sight, some large enough to block 30 per cent of the starlight for days, as in 2008 and 2011. The exact structure of the dust disc could be revealed using high-resolution sub-mm imaging (e.g. with ALMA, as was performed for dipper star EPIC 204 278 916, Scaringi et al. 2016).

Large-scale version of these aperiodic dimmings has been observed as UX Ori-type variables, such as the dips of AA Tau (Bouvier et al. 2003), V1247 Orionis (Caballero 2010), RZ Psc (Kennedy et al. 2017), and V409 Tau (Rodriguez et al. 2015). Similar dips with an unexplained origin have also been seen around older stars, for example, KIC 8462 852 (Boyajian et al. 2016).

The quantity of photometry assembled for PDS 110 here and in Osborn et al. (2017) reveals that dimming events are exceedingly rare, with dips greater than a few per cent in depth occurring during at most 2 per cent of the time. The events are also typically far shallower in magnitude than a typical UX Ori. Therefore, maybe we are seeing such a system at an extremely high viewing angle, at extremely low optical depth, or potentially at a dissipative stage of UX Ori evolution. A more detailed exploration of the high-resolution spectra obtained by UVES and TRES during this campaign may help answer the question of what caused the aperiodic dips of PDS 110 (de Mooij et al., in preparation). Alternatively, the increasing quality of ground-based (e.g. Wheatley et al. 2018; Shappee et al. 2014, etc.) and space-based (Ricker et al. 2010) photometry may reveal more low-amplitude UX Ori systems such as PDS 110.

6 CONCLUSIONS

A large ground-based follow-up campaign of PDS 110 was conducted to search for the predicted eclipse of a dust-encircled massive body postulated to be orbiting within (or above) the dust disc of PDS 110. This included a dozen professional observatories and more than 30 amateur observers. The high-quality photometry recorded spans 10 filters and more than 200 d.

This campaign, and the lack of any eclipse at the predicted transit time, has allowed us to rule out the hypothesis that PDS 110 has a dust-enshrouded companion. This is also backed up by archival photometry from Sonneburg archive, which does not reveal dimmings at the predicted times, radial velocity observations from TRES, which sees no signal from a stellar companion, and UVES observations of PDS 110 during the predicted eclipse, which see no variation in the stellar line profiles. However, the photometric campaign did reveal that PDS 110 does undergo shorter and/or shallower dimming events.

Together, the observations point to a new, aperiodic source of the eclipses, potentially from dust blown above the disc-plane as has been hypothesized for UX Ori-type variables. Future observations of PDS 110 may reveal more such events, and future all-sky surveys may detect more PDS 110-like eclipsers.

ACKNOWLEDGEMENTS

This work is based on observations collected with LCOGT under program LCO2017AB-003, and the European Southern Observatory, Chile under programme 299.C-5047.

This research has used Astropy,[10] a community-developed core PYTHON package for Astronomy (Astropy Collaboration 2013; Price-Whelan et al. 2018) and of Matplotlib (Hunter 2007). We thank our anonymous referee for their helpful comments. We acknowledge with thanks the variable star observations from the AAVSO International Data base contributed by observers worldwide and used in this research. HPO acknowledges support from Centre National d'Etudes Spatiales (CNES) grant 131425-PLATO. MH thanks Frank (Theo) Matthai for assistance with finding the relevant Sonneberg plates in the observatory archive. This work has used the VALD data base, operated at Uppsala University, the Institute of Astronomy RAS in Moscow, and the University of Vienna. EH acknowledges support by the Spanish Ministry of Economy and Competitiveness (MINECO) and the Fondo Europeo de Desarrollo Regional (FEDER) through grant ESP2016-80435-C2-1-R, as well as the support of the Generalitat de Catalunya/CERCA programme. The Joan Oró Telescope (TJO) of the Montsec Astronomical Observatory (OAdM) is owned by the Generalitat de Catalunya and operated by the Institute for Space Studies of Catalonia (IEEC). pt5m is a collaborative effort between the Universities of Durham and Sheffield. The telescope is kindly hosted by the Isaac Newton Group of Telescopes, La Palma. GMK is supported by the Royal Society as a Royal Society University Research Fellow. TB and RWW acknowledge support from the UK Science and Technology Facilities Council (STFC; reference ST/P000541/1). PC acknowledges funding from the European Research Council under the European Union's Seventh Framework Programme (FP/2007-2013) / ERC Grant Agreement n. 320964 (WDTracer). This paper uses observations made at the SAAO. ASAS-SN light curves are primarily funded by Gordon & Betty Moore Foundation under grant GBMF5490. MNG is supported by the STFC award reference 1490409 as well as the Isaac Newton Studentship. LM acknowledges support from the ⟨0:named-content 0:content-type="word-wrap"⟩⟨0:funding-source ⟩Italian Minister of Instruction, University and Research⟨/0:funding-source⟩⟨/0:named-content⟩ (MIUR) through FFABR 2017 fund. LM acknowledges support from the University of Rome Tor Vergata through 'Mission: Sustainability 2016' fund. The NGTS instrument and operations are funded by the University of Warwick, the University of Leicester, Queen's University Belfast, the University of Geneva, the Deutsches Zentrum für Luft- und Raumfahrt e.V. (DLR; under the 'Großinvestition GI-NGTS'), the University of Cambridge and the UK STFC (project reference ST/M001962/1). PJW and RGW acknowledge support by STFC through consolidated grants ST/L000733/1 and ST/P000495/1. ISB, OCW, and RS achknowledge grants CNPQ (305737/2015-5, 312813/2013-9), CNPQ-PIBIC (37815/2016) & FAPESP Proc. 2016/24561-0. TLK acknowledges use of the COAST facility, operated by the Open University.

[10] http://www.astropy.org

REFERENCES

Aizawa M., Masuda K., Kawahara H., Suto Y., 2018, AJ, 155, 206
Ansdell M. et al., 2016, ApJ, 816, 69
Ansdell M. et al., 2018, MNRAS, 473, 1231
Armitage P. J., 2011, ARA&A, 49, 195
Astropy Collaboration, 2013, A&A, 558, A33
Astropy Collaboration, 2018, AJ, 156, 123
Bertin E., Arnouts S., 1996, A&AS, 117, 393
Bouvier J. et al., 1999, A&A, 349, 619
Bouvier J. et al., 2003, A&A, 409, 169
Boyajian T. S. et al., 2016, MNRAS, 457, 3988
Bräuer H.-J., Fuhrmann B., 1992, Stern, 68, 19
Bräuer H.-J., Häusele I., Löchel K., Polko N., 1999, Acta Historica Astronomiae, 6, 70
Buchhave L. A. et al., 2010, ApJ, 720, 1118

Caballero J. A., 2010, A&A, 511, L9
Canup R. M., Ward W. R., 2002, AJ, 124, 3404
Cody A. M., Hillenbrand L. A., 2014, ApJ, 796, 129
Collazzi A. C., Schaefer B. E., Xiao L., Pagnotta A., Kroll P., Löchel K., Henden A. A., 2009, AJ, 138, 1846
Colome J., Ribas I., 2006, in Proc. IAU Symp., Astronomical Data Management. p. 11
Coppejans R. et al., 2013, PASP, 125, 976
Dekker H., D'Odorico S., Kaufer A., Delabre B., Kotzlowski H., 2000, in Iye M., Moorwood A. F., eds, Proc. SPIE Conf. Ser. Vol. 4008, Optical and IR Telescope Instrumentation and Detectors. SPIE, Bellingham, p. 534
de Mooij E. J. W., Watson C. A., Kenworthy M. A., 2017, MNRAS, 472, 2713
Donati J.-F., Semel M., Carter B. D., Rees D. E., Collier Cameron A., 1997, MNRAS, 291, 658
Epchtein N., et al., 1994, Science with Astronomical Near-Infrared Sky Surveys, Springer, 3
Fossey S. J., Waldmann I. P., Kipping D. M., 2009, MNRAS, 396, L16
Fűrész G., 2008, PhD thesis, Univ. Szeged
Ginski C. et al., 2018, A&A, 616, A79
Goranskij V., Shugarov S., Zharova A., Kroll P., Barsukova E. A., 2010, Perem. Zvezdy, 30
Hardy L. K., Butterley T., Dhillon V. S., Littlefair S. P., Wilson R. W., 2015, MNRAS, 454, 4316
Heising M. Z., Marcy G. W., Schlichting H. E., 2015, ApJ, 814, 81
Hippke M. et al., 2017, ApJ, 837, 85
Hunter J. D., 2007, Comput. Sci. Eng., 9, 90
Johnson C. B., Schaefer B. E., Kroll P., Henden A. A., 2014, ApJ, 780, L25
Kafka S., 2016, Observations from the AAVSO International Data base
Kennedy G. M., Kenworthy M. A., Pepper J., Rodriguez J. E., Siverd R. J., Stassun K. G., Wyatt M. C., 2017, R. Soc. Open Sci., 4, 160652
Kenworthy M. A., Mamajek E. E., 2015, ApJ, 800, 126
Kley W., Nelson R. P., 2012, ARA&A, 50, 211
Kochanek C. S. et al., 2017, PASP, 129, 104502
Lang D., Hogg D. W., Mierle K., Blanton M., Roweis S., 2010, AJ, 139, 1782
Magni G., Coradini A., 2004, Planet. Space Sci., 52, 343
Mallonn M. et al., 2018, A&A, 614, A35
Mamajek E. E., Quillen A. C., Pecaut M. J., Moolekamp F., Scott E. L., Kenworthy M. A., Cameron A. C., Parley N. R., 2012, AJ, 143, 72
McCormac J., Pollacco D., Skillen I., Faedi F., Todd I., Watson C. A., 2013, PASP, 125, 548
McCormac J., Skillen I., Pollacco D., Faedi F., Ramsay G., Dhillon V. S., Todd I., Gonzalez A., 2014, MNRAS, 438, 3383
Nemmen R. S., Georganopoulos M., Guiriec S., Meyer E. T., Gehrels N., Sambruna R. M., 2012, Science, 338, 1445
Osborn H. P. et al., 2017, MNRAS, 471, 740
Ricker G. R. et al., 2010, Bull. Am. Astron. Soc., 42, 459
Rodriguez J. E., Pepper J., Stassun K. G., Siverd R. J., Cargile P., Beatty T. G., Gaudi B. S., 2013, AJ, 146, 112
Rodriguez J. E. et al., 2015, AJ, 150, 32
Ryabchikova T., Piskunov N., Kurucz R. L., Stempels H. C., Heiter U., Pakhomov Y., Barklem P. S., 2015, Phys. Scr., 90, 054005
Scaringi S. et al., 2016, MNRAS, 463, 2265
Shappee B. et al., 2014, American Astronomical Society Meeting Abstracts# 223.
Smette A. et al., 2015, A&A, 576, A77
Southworth J. et al., 2009, MNRAS, 396, 1023
Southworth J. et al., 2014, MNRAS, 444, 776
Strassmeier K. G. et al., 2004, Astron. Nachr., 325, 527
Teachey A., Kipping D. M., Schmitt A. R., 2018, AJ, 155, 36
Vanderburg A., Rappaport S. A., Mayo A. W., 2018, AJ, 156, 184
Waagen E. O., 2017, Alert Notice 584: Monitoring of PDS 110 requested to cover upcoming eclipse by exoplanet. Available at: https://www.aavso.org/aavso-alert-notice-584
Ward W. R., Canup R. M., 2010, AJ, 140, 1168
Watson C. A., Dhillon V. S., Shahbaz T., 2006, MNRAS, 368, 637
Wheatley P. J. et al., 2018, MNRAS, 475, 4476
Zacharias N., Urban S. E., Zacharias M. I., Wycoff G. L., Hall D. M., Germain M. E., Holdenried E. R., Winter L., 2004, The Astronomical Journal, 127, 3043

APPENDIX A: OBSERVER OFFSETS

Table A1. Information for each source of *BVRI* photometry during the 2017 observing campaign. Offsets are in relative flux. They are sorted by number of exposures, although this is not necessarily a proxy for photometric quality or observation duration. LCOGT data were re-adjusted such that the median matches the archive value in each band. † denotes those values held fixed. ⋆ demarks where data were initially binned. 'OTHER' denotes AAVSO observers with fewer than 25 observations.

Observatory	$N_{\rm img}(B)$	B Offset	$N_{\rm img}(V)$	V Offset	$N_{\rm img}(R)$	R Offset	$N_{\rm img}(I)$	I Offset
LCOGT 0.4m	–	–	–	–	–	–	–	–
NITES	230	-0.0129 ± 0.001	211	$-0.0074^{+0.0038}_{-0.0018}$	202	-0.0105 ± 0.0008	202	$0.0018^{+0.0012}_{-0.0017}$
LCOGT 1m	215	0†	196	0†	205	0†	–	–
STELLA	134	-0.0081 ± 0.0011	125	$-0.0067^{+0.0013}_{-0.0017}$	–	–	131	-0.0006 ± 0.0012
NGTS	–	–	–	–	–	–	–	–
CAHA	60	$-1.2297^{+0.0023}_{-0.0031}$	65	-0.703 ± 0.0037	63	$-3.1034^{+0.0024}_{-0.0033}$	63	0†
ASAS-SN	–	–	237	-0.0104 ± 0.0011	–	–	–	–
FEG	–	–	137	$0.0493^{+0.0027}_{-0.0013}$	–	–	–	–
TJO	51	$-0.083^{+0.0025}_{-0.002}$	–	–	–	–	45	$0.532^{+0.04}_{-0.076}$
pt5m	18	$-0.0914^{+0.0052}_{-0.0037}$	22	$-0.004^{+0.003}_{-0.004}$	–	–	–	–
SAAO	–	–	11⋆	0.0228 ± 0.0074	10⋆	-0.4365 ± 0.0018	6⋆	-0.2683 ± 0.0011
UCLO	–	–	–	–	9⋆	$-0.0021^{+0.0026}_{-0.0055}$	9⋆	$0.0063^{+0.0018}_{-0.0038}$
AAVSO/LCLC	–	–	1898	$-0.00054^{+0.00092}_{-0.00097}$	–	–	–	–
AAVSO/QULA	365	$-0.0603^{+0.0019}_{-0.0012}$	266	$0.0001^{+0.0023}_{-0.0026}$	338	$-0.3945^{+0.0021}_{-0.0031}$	500	$-0.2745^{+0.0038}_{-0.0022}$
AAVSO/MGW	374	-0.0253 ± 0.0011	369	$0.02156^{+0.00078}_{-0.00052}$	353	$-0.37578^{+0.0007}_{-0.00082}$	366	$-0.2183^{+0.0018}_{-0.0011}$
AAVSO/HMB	455	-0.0451 ± 0.001	555	0.0125 ± 0.001	–	–	439	$-0.2786^{+0.0064}_{-0.0037}$
AAVSO/JM	325	-0.073 ± 0.012	329	0.047 ± 0.008	–	–	–	–
AAVSO/RJWA	–	–	–	–	–	–	–	–
AAVSO/DLM	–	–	281	$0.00703^{+0.00074}_{-0.00078}$	–	–	–	–
AAVSO/HKEB	73	-0.0179 ± 0.0024	73	-0.0065 ± 0.002	76	$-0.354^{+0.003}_{-0.002}$	–	–
AAVSO/PVEA	73	-0.05 ± 0.0019	58	$0.0135^{+0.0013}_{-0.0022}$	–	–	58	-0.2334 ± 0.0014
AAVSO/MXI	47	-0.0676 ± 0.0023	42	0.017 ± 0.002	40	-0.3967 ± 0.0021	39	-0.267 ± 0.0008
AAVSO/BSM	–	–	83	$-0.0213^{+0.0012}_{-0.0022}$	–	–	78	$-0.3358^{+0.0057}_{-0.0027}$
AAVSO/HJW	33	$-0.0725^{+0.0076}_{-0.0055}$	87	$0.0055^{+0.003}_{-0.0038}$	–	–	33	-0.2736 ± 0.0021
AAVSO/BPAD	34	$-0.0492^{+0.0033}_{-0.0044}$	44	$0.0056^{+0.0015}_{-0.0015}$	39	-0.4245 ± 0.002	35	-0.2893 ± 0.0017
AAVSO/DERA	–	–	56	-0.0051 ± 0.003	–	–	57	$-0.2534^{+0.0071}_{-0.0046}$
AAVSO/LMA	–	–	97	$0.0185^{+0.0025}_{-0.0022}$	–	–	–	–
AAVSO/RLUB	–	–	90	$0.0158^{+0.002}_{-0.0026}$	–	–	–	–
AAVSO/FSTC	–	–	83	$0.0113^{+0.0017}_{-0.0053}$	–	–	–	–
AAVSO/LPAC	29	$-0.0477^{+0.002}_{-0.0015}$	41	-0.0182 ± 0.0032	–	–	–	–
AAVSO/KCLA	18	$-0.0544^{+0.0045}_{-0.0031}$	17	0.0001 ± 0.002	17	$-0.4125^{+0.0025}_{-0.0014}$	17	$-0.2825^{+0.0052}_{-0.0016}$
AAVSO/DKS	25	$-0.0182^{+0.0039}_{-0.0046}$	25	$0.014^{+0.0037}_{-0.0026}$	–	–	–	–
AAVSO/BLOC	10	$-0.149^{+0.0043}_{-0.0067}$	20	$-0.0231^{+0.0039}_{-0.0032}$	10	$-0.4063^{+0.0054}_{-0.007}$	–	–
AAVSO/OTHER	3	$-0.0676^{+0.0018}_{-0.004}$	30	$0.0266^{+0.0031}_{-0.0071}$	5	$-0.3999^{+0.0032}_{-0.0055}$	–	–
AAVSO/TTG	9	$-0.0608^{+0.0012}_{-0.0022}$	8	$-0.0006^{+0.0013}_{-0.0017}$	9	$-0.3846^{+0.0016}_{-0.0013}$	12	$-0.2479^{+0.0014}_{-0.0015}$

Table A2. Information for each source of *ugriz* photometry during the 2017 observing campaign. LCOGT data were re-adjusted such that the median matches the archive value in each band.

Observatory	$N_{\rm img}(u)$	u Offset	$N_{\rm img}(g)$	g Offset	$N_{\rm img}(r)$	r Offset	$N_{\rm img}(i)$	i Offset	$N_{\rm img}(z)$	z Offset
LCOGT 0.4m	–	–	405	0†	402	0†	380	0†	378	0†
LCOGT 1m	204	0†	–	–	–	–	–	–	–	–
pt5m	–	–	–	–	23	-0.1771 ± 0.0076	–	–	–	–
AAVSO/RJWA	–	–	164	$-0.9615^{+0.0059}_{-0.0094}$	192	$-0.2654^{+0.0034}_{-0.0042}$	–	–	–	–

[1]*Aix Marseille Université, CNRS, LAM (Laboratoire d'Astrophysique de Marseille) UMR 7326, F-13388 Marseille, France*
[2]*Leiden Observatory, Leiden University, PO Box 9513, NL-2300 RA Leiden, the Netherlands*
[3]*Harvard-Smithsonian Center for Astrophysics, 60 Garden St, Cambridge, MA 02138, USA*
[4]*Department of Physics, University of Warwick, Gibbet Hill Road, Coventry CV4 7AL, UK*
[5]*Centre for Exoplanets and Habitability, University of Warwick, Gibbet Hill Road, Coventry CV4 7AL, UK*
[6]*Las Cumbres Observatory, 6740 Cortona Drive, Suite 102, Goleta, CA 93117, USA*
[7]*School of Physical Sciences, Centre for Astrophysics and Relativity, Dublin City University, Glasnevin, Dublin 9, Ireland*
[8]*Sonneberg Observatory, Sternwarte str 32, D-96515 Sonneberg, Germany*
[9] *UNESP-Sã Paulo State University, Grupo de Dinâmica Orbital e Planetologia, CEP 12516-410 Guaratinguetá, SP, Brazil*
[10]*Acton Sky Portal (Private observatory), Acton, MA, USA*
[11]*Astronomical Observatory, Dipartimento di Scienze Fisiche, della Terra e dell'Ambiente, University of Siena, 53100, Italy*
[12]*Department of Physics and Astronomy, Leicester Institute of Space and Earth Observation, University of Leicester, Leicester, LE1 7RH, UK*
[13]*Centre for Advanced Instrumentation, Department of Physics, University of Durham, South Road, Durham DH1 3LE, UK*
[14]*Department of Astronomy, Stockholm University, Alba Nova University Center, SE-106 91 Stockholm, Sweden*
[15]*Department of Physics, Astronomy, University of Sheffield, Sheffield, S3 7RH, UK*
[16]*Instituto de Astrofísica de Canarias, E-38205 La Laguna, Tenerife, Spain*
[17]*astroLAB IRIS, Verbrandemolenstraat 5, B-8902 Zillebeke, Belgium*
[18]*Astrophysics Group, Keele University, Staffordshire, ST5 5BG, UK*
[19]*UCL Observatory (UCLO), 553 Watford Way, Mill Hill, London NW7 2QS, UK*
[20]*Department of Physics and Astronomy, University College London, Gower St, London WC1E 6BT, UK*
[21]*Astrophysics Group, Cavendish Laboratory, J.J. Thomson Avenue, Cambridge CB3 0HE, UK*
[22]*Vereniging Voor Sterrenkunde (VVS), Brugge, BE-8000, Belgium*
[23]*Montsec Astronomical Observatory (OAdM), Institut d'Estudis Espacials de Catalunya (IEEC), 08034, Barcelona, Spain*
[24]*Physics, Astronomy, York University, Toronto, Ontario L3T 3R1, Canada*
[25]*American Association of Variable Star Observers, 49 Bay State Road, Cambridge, MA 02138, USA*
[26]*Leibniz-Institut für Astrophysik Potsdam (AIP), An der Sternwarte 16, D-14482 Potsdam, Germany*
[27]*Department of Physics, University of Rome Tor Vergata, Via della Ricerca Scientifica 1, I-00133 – Roma, Italy*
[28]*Max-Planck-Institut für Astronomie Königstuhl 17, D-69117 Heidelberg, Germany*
[29]*INAF – Astrophysical Observatory of Turin, Via Osservatorio 20, I-10025 – Pino Torinese, Italy*
[30]*Faculty of Medicine, Medical University of Bialystok, PL-15-089 Bialystok, Poland*
[31]*Department of Physics and Astronomy, Shumen University, 9700 Shumen, Bulgaria*
[32]*Arkansas Tech University, 1701 N. Boulder Ave. Russellville, AR 72801-2222, USA*
[33]*SUPA, School of Physics, Astronomy, North Haugh, St Andrews, KY16 9SS, UK*
[34]*Institute of Planetary Research, German Aerospace Center, Rutherfordstr. 2, D-12489 Berlin, Germany*
[35]*Perth Exoplanet Survey Telescope (PEST), Perth, Australia*
[36]*Astrophysics Research Centre, Queen's University Belfast, Belfast BT7 1NN, UK*

This paper has been typeset from a TEX/LATEX file prepared by the author.